Ab-initio Studies of the Electronic Structures of the Hexavalent Uranium Compounds K_2UO_4 and Na_4UO_5

Samir F. Matar[a,b]

[a] CNRS, ICMCB, UPR 9048, F-33600 Pessac, France

[b] Université de Bordeaux, ICMCB, UPR 9048, F-33600 Pessac, France

Reprint requests to Samir F. Matar. E-mail: matar@icmcb-bordeaux.cnrs.fr

Z. Naturforsch. **2014**, *69b*, 109 – 115 / DOI: 10.5560/ZNB.2014-3280
Received October 8, 2013

Band theoretical results within the density functional theory are reported for the uranates K_2UO_4 and Na_4UO_5. The two structures are differentiated respectively by uranyl and reverse uranyl-type short U–O distances characterizing the UO_6 octahedra, as also reflected by larger compressibility and stability of the potassium-based uranate derived from energy-volume equations of states and the cohesive energy. A larger ionic character of Na_4UO_5 is inferred from comparative Bader charge analyses. The two uranates are insulators with a larger band gap and less extended valence and conduction bands for Na_4UO_5. Chemical bonding shows major interactions for U–O *versus* Na,K–O and is further differentiated as a function of the distances. The band structure results confirm the hexavalent character of the uranium atoms.

Key words: Alkali Uranates, Hexavalent Uranium, Equation of State, DFT, VASP, ASW, Bader, COOP

Introduction

Binary and ternary uranium oxides have been well known since the first half of last century and have been characterized mainly with regard to their crystal structures [1 – 3]. For technology-relevant systems such as nuclear fuel compounds and for stabilized storage media of nuclear wastes, a detailed knowledge of the physical properties and chemical bonding is useful at both the fundamental and application levels.

Besides data from experimental investigations, information on the electronic band structure, on the equation of state (EOS) [4] as well as on the properties of chemical bonding can be obtained using quantum-mechanical computational methods. Despite its basic principle of one electron theory, as opposed to many body theories, the density functional theory DFT [5, 6] is nowadays the established framework for most studies. *Ab-initio* investigations were undertaken by others and by us for uranium(IV) oxide UO_2 [7, 8] and for AUO_4 (A = Ca, Cd) compounds [9, 10] as well as for UO_2CO_3 [11] aiming at establishing structure-properties relationships. The hexavalent uranium-based oxides are characterized by the linear uranyl cation UO_2^{2+}. This is also found in the recently prepared alkali uranates K_2UO_4 and Na_4UO_5 prepared by the zur Loye group using KOH and NaOH hydroxide flux methods and characterized by X-ray diffraction [12]. The two oxides crystallize in body-centered tetragonal space groups and are characterized by corner-sharing irregular UO_6 octahedra (Fig. 1). From Tables 1 and 2, providing the experimental structural specifications, it appears that the difference between K_2UO_4 and Na_4UO_5 is mainly in the U–O distances within the octahedra. By differentiating shorter distances for O2 (red spheres) *versus* longer ones for O1 (blue spheres) for the sake of clarity, there are four uranyl-type U–O2 bonds in the sodium uranate, while in the potassium uranate two of these bonds lie along the crystallographic c axis. This leads to a labeling of K_2UO_4 as 'uranyl-based' and for Na_4UO_5 as 'reverse uranyl'-based. It is expected that such peculiar features may have consequences on the electronic and mechanical properties which are investigated herein by establishing the energy-volume (E,V) equations of states (EOS), the trends in charge transfer as well as the atom-resolved densities of states PDOS and qualitative chemical bonding properties based on overlap populations.

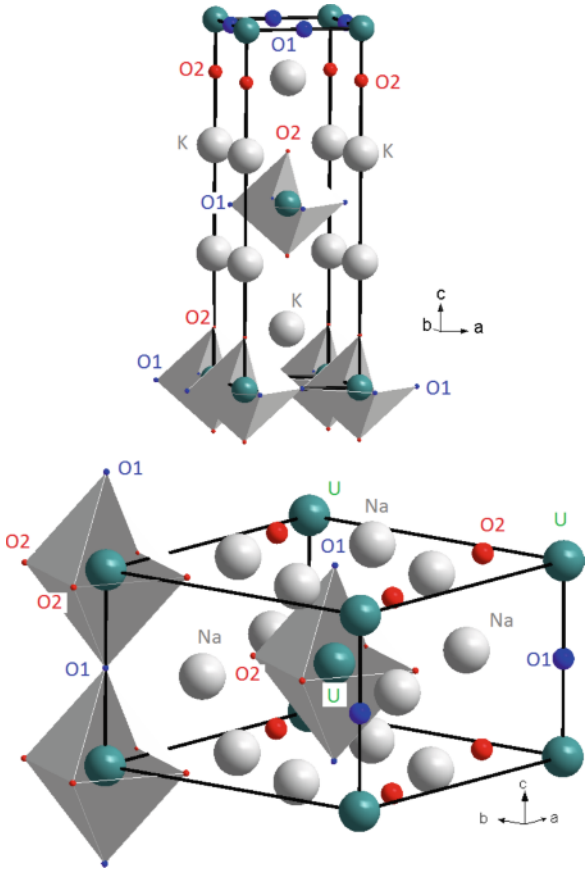

Fig. 1 (color online). Sketches of the structures of K_2UO_4 (top) and Na_4UO_5 (bottom) stressing the different oxygen substructures (O2 relates to uranyl-like shorter U–O distances).

Table 1. Lattice specifications of K_2UO_4 with U at Wyckoff position 2*a* (0, 0, 0) and O1 at Wyckoff position 4*c* ($^1/_2$, 0, 0).

K_2UO_4 *I*4/*mmm* (# 139)	Experimental [12]	Calculated
a (Å)	4.332	4.35
c (Å)	13.138	13.38
V (Å^3)	246.56	253.18
Atoms		
K ($^1/_2$, $^1/_2$, *u*) 4*e*	$u = 0.1507$	$u = 0.152$
O1 (0, 0, *v*) 4*e*	$v = 0.1456$	$v = 0.144$
Distances (Å)		
U–O2/U–O1	1.92/2.16	1.95/2.18
K–O2/K–O1	2.93/3.06	2.98/3.08
K–U	3.65	3.69

Table 2. Lattice specifications of Na_4UO_5 with U at Wyckoff position 2*a* (0, 0, 0) and O2 at Wyckoff position 2*b* (0, 0, $^1/_2$).

Na_2UO_5 *I*4/*m* (# 87)	Experimental [12]	Calculated
a (Å)	7.517	7.40
c (Å)	4.632	4.61
V (Å^3)	261.78	252.44
Atoms		
Na (*u*, *v*, 0) 8*h*	$u = 0.1960$	$u = 0.195$
	$v = 0.4043$	$v = 0.405$
O2 (*u*′, *v*′, 0) 8*h*	$u' = 0.2563$	$u' = 0.259$
	$v' = 0.0777$	$v' = 0.079$
Distances (Å)		
U–O1/U–O2	2.32/2.02	2.34/2.04
Na–O1/Na–O2	2.70/2.40	2.68/2.40
Na–U	3.38	3.39

Computational Framework

Within DFT, two methods were used complementarily:

The VASP (Vienna *ab-initio* simulation package) code [13, 14] allows for geometry optimization and establishing EOS and charge transfer trends. The method implements projector augmented wave (PAW) [14, 15] potentials. We used them as built within the generalized gradient approximation (GGA) [16] DFT exchange correlation XC functional. Preliminary test calculations with the local density approximation [17] PAW-LDA gave smaller unit cell volumes with respect to the experiment. Besides being more accurate than ultra-soft PP's, PAW potentials treat properly the *f* orbitals. The valence states used in the construction of the PAW potentials are: Na ($2p^6\ 3s^1$); K ($3p^6\ 4s^1$); U ($5s^2\ 5p^6\ 5f^3\ 6d^1\ 7s^2$) and O ($2s^2\ 2p^4$). By including semi-core states (for Na, K), a better account for the electronic structure is obtained. The optimization of the structural parameters is performed until the forces on the atoms are less than 0.02 eV Å^{-1}, and all stress components are below 0.003 eV Å^{-3}. Calculations are converged at an energy cut-off of 500 eV for the plane-wave basis set. Brillouin zone (BZ) integrals are approximated [18] using **k**-point grids with a starting mesh of $4 \times 4 \times 4$ up to $8 \times 8 \times 8$ for best convergence and relaxation to zero strains. We used the atoms in molecules theory (AIM) approach [19] developed by Bader who devised an intuitive way of splitting molecules into atoms as based purely on the electronic charge density. Typically in chemical systems, the charge density reaches a minimum between atoms, and this is a natural region to separate them from each other. Such an analysis can be useful when trends between similar compounds are examined; however, they do not constitute a tool for evaluating absolute ionizations.

All-electron calculations, equally with the GGA XC functional, were carried out for a full description of the electronic structure and of the properties of chemical bonding, using the full potential scalar-relativistic augmented spherical wave (ASW) method [20, 21]. In the minimal ASW basis set, we chose the outermost shells to represent the valence states, and the matrix elements were constructed using partial waves up to $l_{\max}+1=4$ for U, and $l_{\max}+1=2$ for Na, K and O. Self-consistency was achieved when charge transfers and energy changes between two successive cycles were below 10^{-8} and 10^{-6} eV, respectively. BZ integrations were performed using the linear tetrahedron method within the irreducible wedge. In order to optimize the basis set, additional augmented spherical waves were placed at carefully selected interstitial sites (IS). Besides the site-projected density of states, we discuss qualitatively the pair interactions based on the overlap population analysis with the crystal orbital overlap population (COOP) [22]. In the plots, positive, negative, and zero COOP indicate bonding, antibonding, and non-bonding interactions, respectively.

Note on the effects of enhanced correlation

It can be argued that using an electron gas-based functional in the present calculations might constitute a drawback in accounting for an actinide-based compound. For a check we have carried out additional calculations by introducing the Hubbard repulsive parameter U, leading to the so called GGA$+U$ approach. With values used by Freyss et al. for the study of UO_2 and its defect structure, $U=4.5$ eV and $J=0.5$ eV [23], the resulting DOSs were shown to exhibit the same general features (Fig. 2). The difference of the band gap increases by ~ 0.3 eV leading to

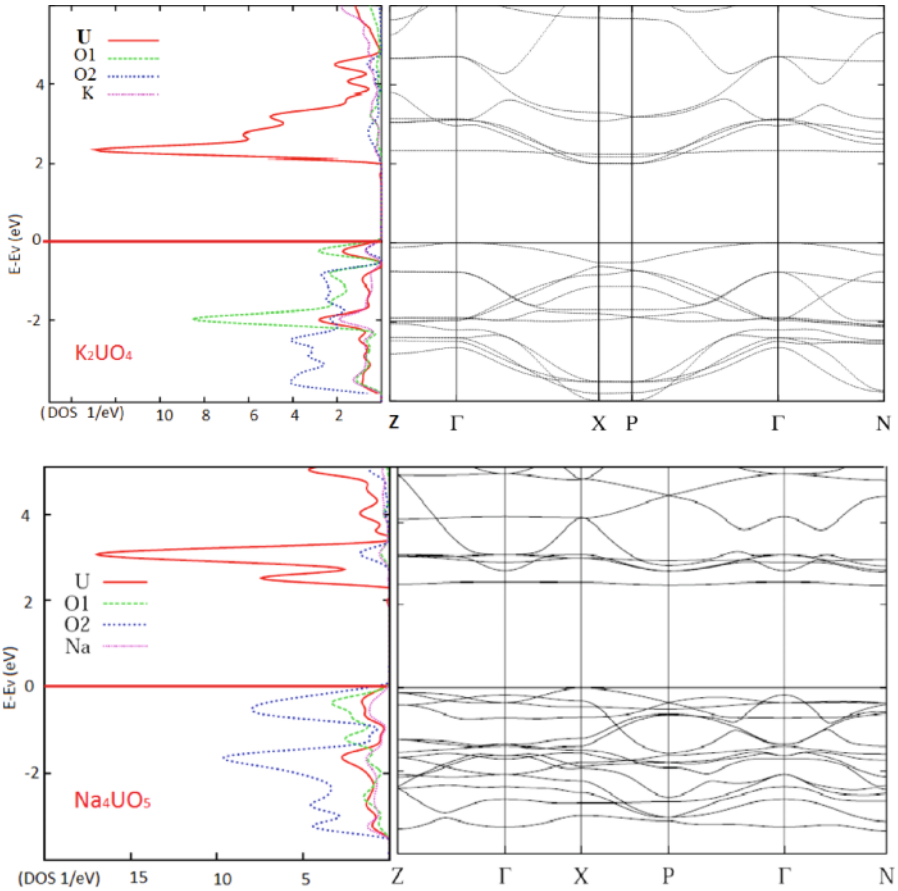

Fig. 2 (color online). Band structures and site-projected DOS of K_2UO_4 (top) and Na_4UO_5 (bottom).

more insulating systems. The localization of the uranium f bands in the CB is also the same. This probably arises from the fact that in the two compounds the empty f subshell of hexavalent uranium is involved (U^0: [Rn]$5f^3 5d^1 7s^2 \rightarrow U^{6+}$: [Rn]$5f^0 5d^0 7s^0$) (*cf.* band structures). Therefore, the theoretical treatment using a scalar-relativistic calculation scheme and the GGA XC functional stands correctly.

Results and Discussion

Projector Augmented Wave (PAW) calculations

Geometry optimization and charge analysis

Starting from the experimental data of Table 1, a full geometry relaxation was carried out with PAW-GGA. In the right hand side columns of Tables 1 and 2 giving the relaxed lattice parameters, there can be observed some deviation *versus* the experimental data. The volume change does not follow the same trend in the two compounds. The $\sim$10 Å^3 larger volume calculated for K_2UO_4 is a deviation which can be assigned to the use of the GGA XC functional known to be underbinding, *i. e.* underestimating the lattice spacing. However, the volume is calculated smaller by the same amount for Na_4UO_5, which is not attributable to the DFT functional in use but rather to the different chemical nature of the compound. Nevertheless, $\Delta V/V$ is small enough ($\sim 4\,\%$) to give confidence in the results of the calculations which give values of internal atomic coordinates and interatomic distances in good agreement with the experiment.

Trends in charge transfers

We first analyzed the charge density (CHGCAR) using Bader's AIM theory [20]. The results of computed charges (Q) are such that they lead to neutrality when the respective multiplicities are accounted for (*cf.* Tables 1 and 2). The obtained values are:

$$\begin{aligned} K_2UO_4:\ & Q(\mathrm{U}) = +2.858; \quad Q(\mathrm{K}) = +0.864; \\ & Q(\mathrm{O1}) = -1.165; \quad Q(\mathrm{O2}) = -1.128. \\ Na_4UO_5:\ & Q(\mathrm{U}) = +2.737; \quad Q(\mathrm{Na}) = +0.860; \\ & Q(\mathrm{O1}) = -1.285; \quad Q(\mathrm{O2}) = -1.223. \end{aligned}$$

Uranium does not ionize to the hexavalent state; neither does oxygen become O^{2-} because the ionocovalent character prevails in the solid. Only Na and K are calculated at a nearly monovalent state with a charge close to 1. Although uranium has a larger electron transfer in K_2UO_4 than in Na_4UO_5, the overall electron transfer from cationic species (U, K, Na) to anionic oxygen is larger in Na_4UO_5. This result suggests a slightly more ionic character of the sodium compound, likely due to the two times larger number of Na cations per formula unit (FU).

Cohesive energies

The cohesive energies are obtained from the differences between the total energy of the compounds and that of the atomic constituents Na, K, U with their ground state structures, and dioxygen in a large cubic box with $a = 10$ Å. In PAW-GGA calculations, the following values are obtained: $E(\mathrm{Na}) = -1.32$ eV per atom, $E(\mathrm{K}) = -1.012$ eV per atom, and $E(\mathrm{U}) = -11.00$ eV and $E(\mathrm{O_2}) = -11.206$ eV per O_2. From the total electronic en-

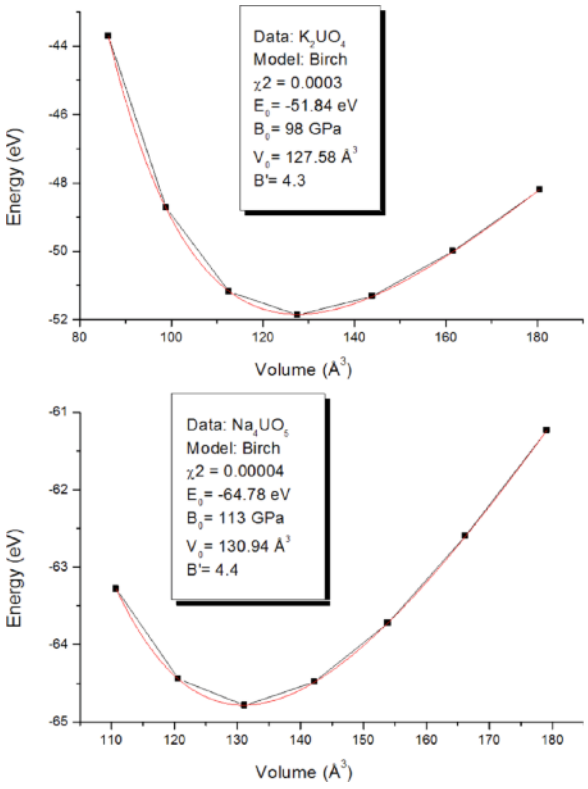

Fig. 3 (color online). Energy-volume curves of K_2UO_4 (top) and Na_4UO_5 (bottom) and parameters of quadratic fit from the Birch EOS given in the inserts.

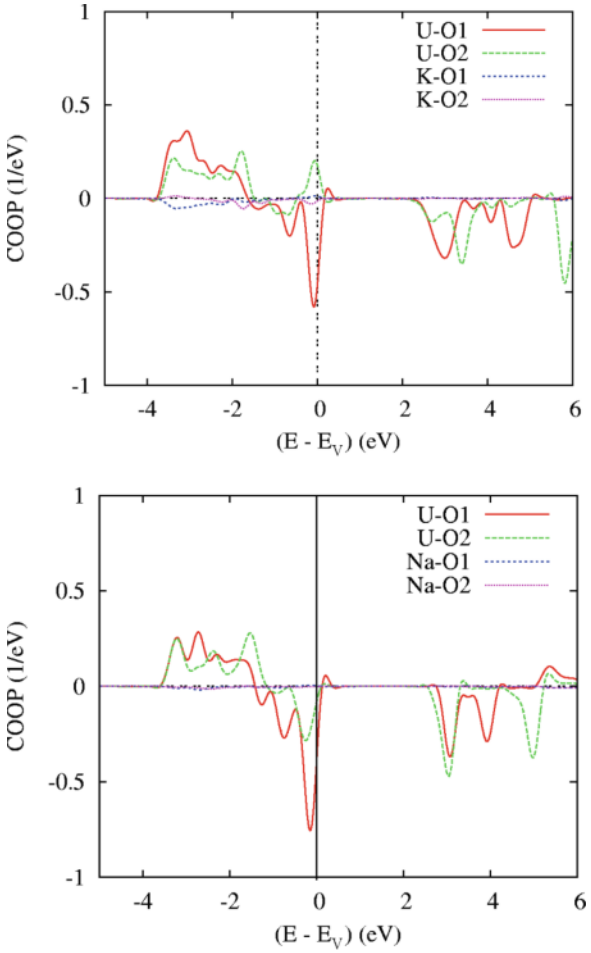

Fig. 4 (color online). Chemical bonding based on the COOP criterion in K_2UO_4 (top) and Na_4UO_5 (bottom).

ergies given in Fig. 2, the resulting cohesive energies are: $E_{\text{coh.}}(K_2UO_4) = -2.343$ eV per atom and $E_{\text{coh.}}(Na_4UO_5) = -2.048$ eV per atom. The slightly less cohesive character of the latter compound can have different origins pertaining to the overall smaller lattice spacing (*cf.* Tables 1, 2) and to the relative magnitudes of bonding/antibonding pair interactions within the valence band, which is shown in Fig. 4 to display larger bonding positive COOP intensities in K_2UO_4.

Energy-volume EOS

The geometry relaxation results can be assessed further from plotting the energy-volume $E_i = f(V_i)$ curves for discrete sets of $V_i < V_{\text{opt.}}$ and $V_i > V_{\text{opt.}}$ being the geometry optimized volume. From $E_i = f(V_i)$ curves which have a quadratic like shape, the corresponding EOS can be established. The curves are shown in Fig. 3 for the two phases. The energy and volume scales correspond to one formula unit (FU) explicitly calculated insofar as the two compounds belong to space groups with I centering. The two curves exhibit quadratic shapes and can be fitted by a Birch EOS [4] up to the 3$^{\text{rd}}$ order expressed as follows:

$$E(V) = E_0(V_0) + \frac{9}{8}V_0B_0\left[(V_0/V)^{2/3} - 1\right]^2 + \frac{9}{16}B_0(B' - 4)V_0\left[(V_0/V)^{2/3} - 1\right]^3$$

In this equation E_o, V_o, B_o and B' are the equilibrium energy, the volume, the bulk modulus and its pressure derivative, respectively. The obtained values are displayed in the insets of Fig. 3. There is a better agreement with experiment for the volume magnitudes. The pressure derivative of the bulk modulus B' is ~ 4, a value usually encountered for oxides [24]. χ^2 indicates the goodness of fit. Relevant results are the B_o values which indicate that the sodium uranate is harder than the potassium uranate, although one would expect the opposite from the volume magnitudes: *i. e.* the larger the volume the more compressible the compound should be. The discrepancy should therefore have a different origin related with the local environments of the UO_6 octahedra as already noted in the introduction and sketched in Fig. 1: There are 4 short equatorial U–O2 distances (red O2) and two longer axial U–O1 distances in Na_4UO_5 (reverse uranyl) whereas a (straight) uranyl unit O2–U–O2 orientated along the c axis and 4 longer distances U–O1 are observed in K_2UO_4. This may explain why Na_4UO_5 is harder.

All-electrons calculations

Electronic band structure and site-projected density of states

Using the experimental structural data (Tables 1 and 2), scalar relativistic calculations were carried out with the ASW method for a detailed analysis of the atom-resolved electronic density of states (PDOS) and the overlap population with the COOP criterion.

At self consistency, charge transfers with magnitudes close to the ones obtained above are observed from uranium and the alkali elements towards the oxygen atoms on the one hand as well as to the interstitial spheres (IS) on the other hand. These trends, not supporting the hexavalent character of uranium, are indirectly obtained from the electronic band structure together with the corresponding site-projected density of states PDOS given in Fig. 2.

The O($2s$) states lying at low energy are not shown. Both panels exhibit insulating characteristics insofar that a band gap close to 2 and ~ 2.2 eV is observed in the potassium and sodium compounds, respectively. The valence band VB below E_V is dominated by itinerant oxygen states (mainly p-character) and uranium states (d, f) which mix leading to the chemical bonding detailed in the next section. However the major part of the uranium f states is found in the conduction band CB due to low filling of U($5f$) levels in the atomic state. The slightly more pronounced ionic behavior of Na_4UO_5 deducted from the charge transfer magnitudes leads to a narrower VB and sharper uranium states in the CB, as well as to a slightly larger band gap with respect to the potassium compound. Visual inspection of the VB shows different shapes of O1 *versus* O2, thus indicating different bonding characteristics for U. The PDOS peak at ~ -2 eV characterizes O2 and points to preferential U–O2 bonding. This shows up explicitly in the chemical bonding analysis below. The DOS features are mirrored by the band structures plotted along the major lines of the Brillouin zones of the body centered tetragonal Bravais lattices. This is especially illustrated for the band dispersion, which is larger for the potassium uranate than for the sodium uranate.

Counting the bands in the VBs provides 12 bands for K_2UO_4 and 15 bands for Na_4UO_5. Disregarding the O($2s$) states at low energy, these bands accommodate, respectively 24 (K_2UO_4) and 30 (Na_4UO_5) valence electrons per FU. This corresponds to the filling of O($2p$) states for 4 oxygen atoms in K_2UO_4 and for 5 oxygen atoms in Na_4UO_5. The bands of U, Na and K are all empty and found within the CBs. An ionic description of the compounds is thus reached for Na^+ and K^+ and in particular for U^{6+} cations ([Rn]$5f^0 5d^0 7s^0$).

Chemical bonding

The electronic structures can be further illustrated by the chemical bonding properties using the COOP criterion for pair interactions [22]. In order to enable trends of bond strengths, one atom of each kind is accounted for in the plots shown in Fig. 4. In both panels the U–O bonding prevails over Na–O and K–O bonding for the two sites of oxygen. This is expected from the characterization of the alkali elements by delocalized, non directional, s valence states. The U–O interaction is differentiated between the two oxygen sites O1 (non-uranyl) and O2 (uranyl-like) from ~ -4 eV up to E_V. In K_2UO_4 equatorial U–O1 COOPs are more intense than axial U–O2 COOPs, but they present antibonding character with largely negative COOP magnitudes towards the top of the VB. This is opposite to U–O2 which shows more bonding character and a relatively intense COOP peak at -2 eV, *i. e.* at the same energy as the O2-PDOS in Fig. 2. This feature as well as the antibonding characters at the top of the VB are also present in the bottom panel of Na_4UO_5 and suggest four U–O2 bonds. However, these equatorial uranyl-like U–O2 interactions become antibonding at the top of the VB. The overall larger bonding magnitudes in the potassium uranate reflect the larger cohesive energy calculated above.

Conclusion

In this work *ab initio* results on the electronic structures of the uranates K_2UO_4 and Na_2UO_5 have been presented based on DFT computations. Both compounds are insulators with $\sim$2 eV band gap reflecting indirectly the hexavalent state of uranium. From energy-volume equations of states, the sodium uranate is harder and less compressible than the potassium compound in spite of its larger volume due to two short U–O connectivities thanks to the 'reverse uranyl' character of Na_2UO_5. Concomitantly, the straight uranate K_2UO_4 is found slightly more cohesive thanks to smaller overall interatomic spacing and stronger bonding of the valence band as inferred from overlap population analysis.

Acknowledgement

Discussions on the topic of uranates with Prof. Michel Pouchard of the French Academy of Science are gratefully acknowledged.

Computational facilities were provided by the Université de Bordeaux on main frame computers of MCIA. Support from the Conseil Régional d'Aquitaine is acknowledged.

[1] W. H. Zachariasen, *Acta. Crystallogr.* **1948**, *1*, 265.
[2] C. L. Christ, J. R. Clark, H. T. Evans, Jr., *Science* **1955**, *121*, 472.
[3] W. H. Zachariasen, *Acta. Crystallogr.* **1948**, *1*, 281.
[4] F. Birch, *J. Geophys. Res.* **1978**, *83*, 1257.
[5] P. Hohenberg, W. Kohn, *Phys. Rev. B* **1964**, *136*, 864.
[6] W. Kohn, L. J. Sham, *Phys. Rev. A* **1965**, *140*, 1133.
[7] H. Y. Geng, Y. Chen, Y. Kaneta, M. Kinoshita, *Phys. Rev. B* **2007**, *75*, 054111.
[8] R. A. Evarestov, A. I. Panin, A. V. Bandura, *Russ. J. Gen. Chem.* **2008**, *78*, 1823.
[9] S. F. Matar, G. Demazeau, *J. Solid State Chem.* **2009**, *182*, 2678.
[10] S. F. Matar, *Chem. Phys. Lett.* **2009**, *476*, 213.
[11] S. F. Matar, *Chem. Phys.* **2010**, *372*, 46.
[12] I. P. Roof, M. D. Smith, H.-C. zur Loye, *J. Cryst. Growth* **2010**, *312*, 1240.
[13] G. Kresse, J. Furthmüller, *Phys. Rev. B* **1996**, *54*, 11169.
[14] G. Kresse, J. Joubert, *Phys. Rev. B* **1999**, *59*, 1758.
[15] P. E. Blöchl, *Phys. Rev. B* **1994**, *50*, 17953.
[16] J. Perdew, K. Burke, M. Ernzerhof, *Phys. Rev. Lett.* **1996**, *77*, 3865.
[17] D. M. Ceperley, B. J. Alder, *Phys. Rev. Lett.* **1980**, *45*, 566.
[18] H. J. Monkhorst, J. D. Pack, *Phys. Rev. B* **1976**, *13*, 5188.
[19] R. Bader, *Chem. Rev.* **1991**, *91*, 893.
[20] A. R. Williams, J. Kübler, C. D. Gelatt, *Phys. Rev. B* **1979**, *19*, 6094.
[21] V. Eyert, *The Augmented Spherical Wave Method – A Comprehensive Treatment*, Lect. Notes Phys., Vol. 719, Springer, Berlin, Heidelberg, **2007**.
[22] R. Hoffmann, *Angew. Chem., Int. Ed. Engl.* **1987**, *26*, 846.
[23] M. Freyss, J. Durinck, B. Dorado, Colloque 3M, 2 – 3 June **2008**, Saclay, France (unpublished).
[24] S. F. Matar, G. Demazeau, M. H. Möller, R. Pöttgen, *Chem. Phys. Lett.* **2011**, *508*, 215.